# FFT based iterative schemes for composite conductors with uniform boundary conditions

Vincent Monchiet, Guy Bonnet

# FFT based iterative schemes for composite conductors with uniform boundary conditions

V. Monchiet *, G. Bonnet

*Univ Gustave Eiffel, Univ Paris Est Creteil, CNRS, MSME UMR 8208, F-77454 Marne-la-Vallée, France*

ARTICLE INFO

*Keywords:*
Homogenization
Composites
Conductivity
FFT
Boundary conditions

ABSTRACT

In the present paper, we extend the FFT method to deal with the homogenization problem of composite conductors with uniform boundary conditions. The principle of the approach consists of applying a transformation to build a periodic problem from the solution with uniform boundary conditions. It is shown that the related periodic problem must be applied to an extended domain obtained by mirror symmetry of the unit cell. The conductivity equation must then be solved on this extended domain under an applied periodic polarization field as a loading parameter. Illustrations are provided and the effective conductivity obtained with FFT is compared to finite element solutions to validate the approach. The proposed method can be applied to microstructure geometries of all kinds, including cells obtained through imaging devices.

## 1. Introduction

The determination of the effective properties of composite conductors involves the resolution of the heat equation with specific conditions at the boundary of the considered unit cell. Three kinds of boundary conditions are commonly used: periodic boundary conditions, uniform temperature gradient conditions (Dirichlet type), and uniform flux conditions (Neumann type). Uniform boundary conditions were introduced in the context of random composites and are due to the pioneering works by Hill (1952, 1963) and Kröner (1953, 1958). Alternatively, in the field of asymptotic homogenization methods (see Auriault and Sanchez-Palencia (1977), Sanchez-Palencia (1980) and Bensoussan et al. (1978)), the effective properties of the composite are determined by solving the unit cell problem with periodic boundary conditions. While these boundary conditions have been introduced for specific microstructures, the periodic conditions can be applied at the boundary of a unit cell of a random microstructure and uniform boundary conditions to periodic composites. This raises fundamental questions about the comparison between the effective properties computed with these different kinds of boundary conditions. Also, the definition of the representative volume element over which the boundary conditions are applied has been addressed in many works (Huet, 1990; Hazanov and Huet, 1994; Kanit et al., 2003), but such problems are not central in the present work.

In this paper, we address the question of solving the unit cell problem with uniform boundary conditions. This question has been the subject of many recent studies in the case of composite elasticity. For instance, Gélébart (2020) proposed to consider the problem with Dirichlet boundary conditions using the FFT method by embedding the unit cell in a larger domain to apply periodic boundary conditions. To et al. (2021) addressed the more general problem of Dirichlet and Neumann boundary conditions. Other approaches consist of applying a mirror transformation to the original unit cell (Wiegmann, 1999; Grimm-Strele and Kabel, 2021). Wiegmann (1999) provides a general method for solving homogeneous cells with arbitrary Dirichlet and Neumann boundary conditions with Fourier series. However, it does not deal with the problem of composites and the FFT method of Moulinec and Suquet (1994, 1998). Grimm-Strele and Kabel (2021) extend the FFT method of Moulinec and Suquet to deal with mixed boundary conditions in the case of elasticity but fail to deal with the Dirichlet and Neumann boundary conditions. In the present paper we deal with the thermal conductivity problem whose equations are close to elasticity but for which transformations have been identified to deal with uniform (Dirichlet and Neumann) boundary conditions. In fact, the principle of the mirrors method is older and can be attributed, for instance, to Timoshenko and Woinowsky-Krieger (1959) who considered periodic alternated loadings to solve the problem of rectangular plates. It should also be noted that in the case of a symmetric microstructure, it can be shown that solving the periodic boundary conditions can be accomplished by applying known (mixed) boundary conditions (Bornert et al., 2006).

In this paper, we propose to handle the problem with Dirichlet and Neumann conditions for anisotropic composite conductors. The

* Corresponding author.
*E-mail address:* vincent.monchiet@univ-eiffel.fr (V. Monchiet).

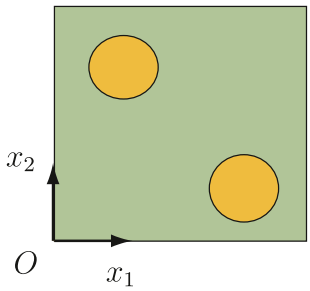


**Fig. 1.** Unit cell of the composite conductor.

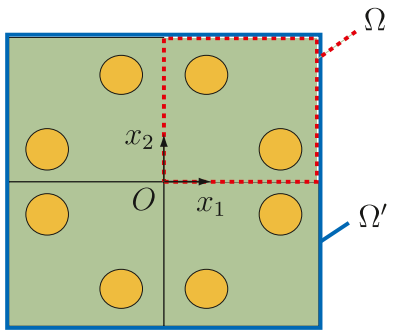


**Fig. 2.** Extended unit cell of the composite conductor.

method is based on the mirror transformation already considered by Wiegmann (1999) and Grimm-Strele and Kabel (2021) but introduce new transformation for the temperature field to derive a periodic problem on a larger domain. By doing so, it is shown that the classic FFT method can be applied considering new appropriate loadings fields. The advantage of our proposed method is that it can easily be implemented with existing home-made FFT codes without major modifications. More specifically, we extend the primal approach of Moulinec and Suquet (1994, 1998), the dual approach (Bhattacharya and Suquet, 2005; Bonnet, 2007), and the polarization method (Monchiet and Bonnet, 2012) to deal with the Dirichlet and Neumann problems. Illustrations and comparisons with FE solutions are provided to validate the approach.

## 2. Statement of the problem

We consider a unit cell of a composite and we assume that this cell is parallelepipedic (rectangular for 2D problems) and we denote by $L_1, L_2, L_3$ its dimensions along each space directions of the cartesian frame $(O, x_1, x_2, x_3)$. The center of the cartesian frame, denoted "O", is located at the left bottom corner of the unit cell $\Omega$ as shown in Fig. 1.

The homogenized conductivity properties of a composite material are classically determined by solving the set of partial differential equations:

$$\mathrm{div}(\boldsymbol{\sigma}) = 0 \tag{1}$$

$$\boldsymbol{\sigma} = \boldsymbol{K}(\boldsymbol{x}).\boldsymbol{\varepsilon} \tag{2}$$

$$\boldsymbol{\varepsilon} = \nabla u \tag{3}$$

with appropriate boundary conditions. Three kind of conditions are conventionally applied to the unit cell:

- Uniform temperature gradient at the boundary (Dirichlet boundary condition):

$$u = \boldsymbol{E}.\boldsymbol{x}, \quad \forall \boldsymbol{x} \in \partial\Omega \tag{4}$$

- Uniform flux at the boundary (Neumann boundary condition):

$$\boldsymbol{\sigma}.\boldsymbol{n} = \boldsymbol{\Sigma}.\boldsymbol{n}, \quad \forall \boldsymbol{x} \in \partial\Omega \tag{5}$$

- Periodic boundary conditions:

$$u - \boldsymbol{E}.\boldsymbol{x} \text{ periodic}, \quad \boldsymbol{\sigma}.\boldsymbol{n} \text{ antiperiodic} \tag{6}$$

The FFT method is based on Fourier series discretization, the periodic boundary conditions are then implicitly satisfied by the considered space of discretization functions. However the method cannot be applied to the two other kinds of boundary conditions. For instance, with the Dirichlet condition, the total temperature field can be decomposed into two parts: (i) a temperature associated with the applied temperature gradient $\boldsymbol{E}$ that is $\boldsymbol{E}.\boldsymbol{x}$, (ii) a fluctuation $v = u - \boldsymbol{E}.\boldsymbol{x}$ that is null at the boundary of the RVE. This field $v$ is then periodic and can be represented along Fourier series. However, the related normal flux $\boldsymbol{\sigma}.\boldsymbol{n}$ takes values on the boundary that are obtained from the solution of the Dirichlet problem and have no reason to be antiperiodic for this kind of boundary conditions. Similarly, in the case of the Neumann condition at the boundary, the value of temperature at the boundary has no reason to be periodic.

## 3. Dirichlet problem

### 3.1. Extension of the domain

We first deal in this section with the conductivity problem related to Dirichlet boundary condition. As already explained, the difficulty arises from the fact that the flux is arbitrary on the boundary of the cell while the FFT method is restricted to problems with the antiperiodicity for the normal flux. The principle of the approach is to solve a complementary problem over a larger unit cell obtained with mirror transformation. Considering the initial unit cell $\Omega = [0, L_1]\times[0, L_2]\times[0, L_3]$, we build a new cell $\Omega'$ by reflexion with respect to the three orthogonal planes $Ox_1x_2$, $Ox_1x_3$ and $Ox_2x_3$ of the cartesian frame (see Fig. 2 for the representation of the extended cell $\Omega'$ in the 2D case).

Let us denote by $I_\alpha(\boldsymbol{x})$, for $\alpha = 1, 2$ and $\forall \boldsymbol{x} \in \Omega$, the characteristic functions of the phases : $\alpha = 1$ for the matrix and $\alpha = 2$ for the inclusions. The characteristic function $I_\alpha(\boldsymbol{x})$ is equal to 1 in the phase $\alpha$ and is null outside. The characteristic function over the extended domain $\Omega'$ is given by:

$$I'_\alpha(\boldsymbol{x}) = I_\alpha(\boldsymbol{S}.\boldsymbol{x}) \tag{7}$$

in which $I'_\alpha(\boldsymbol{x})$ is defined over the extended domain $\Omega'$ while $I_\alpha(\boldsymbol{x})$ only lies in $\Omega$. The components of $\boldsymbol{S}$ in the cartesian frame are:

$$\boldsymbol{S} = \begin{pmatrix} s_1 & 0 & 0 \\ 0 & s_2 & 0 \\ 0 & 0 & s_3 \end{pmatrix} \tag{8}$$

in which $s_i = \mathrm{sign}(x_i)$ for $i = 1, 2, 3$.

### 3.2. Compatibility equation

Denoting by $v = u - \boldsymbol{E}.\boldsymbol{x}$ the fluctuation in the Dirichlet problem, we introduce $v'(\boldsymbol{x})$ defined by:

$$v'(\boldsymbol{x}) = s_1 s_2 s_3 v(\boldsymbol{S}.\boldsymbol{x}), \quad \forall \boldsymbol{x} \in \Omega' \tag{9}$$

Again, $v'(\boldsymbol{x})$ is defined over $\Omega'$ while $v(\boldsymbol{x})$ only lies in $\Omega$. With the introduction of $v'$, it is shown in the next that it is possible to introduce a flux that is $\Omega'$-antiperiodic while the flux related to $v$ is not $\Omega$-antiperiodic.

Because $v$ is null at the boundary of $\Omega$, $v'$ is null at the boundary of each individual cells (the original cell $\Omega$ and its image by the reflexion). As a consequence, $v'$ is continuous from one individual cell to another. In addition, the temperature $v'$ is $\Omega'$-periodic because it is null at the boundary of $\Omega'$ and has a null volume average over $\Omega'$ (due to the coefficient $s_1 s_2 s_3$ behind $v$ in Eq. (9) whose value alternates between 1 and $-1$). Note that on the interface between the individual unit cells, the continuity of the flux at the interface between individual cells is also

equivalent to the continuity of the normal gradient because the material has the same conductivity at both side of the interface. This is due to the mirror symmetry transformation applied to the original cell. Moreover, the temperature being continuous at the interface between individual cells, the tangential components of the gradient of temperature is also continuous. Finally, the normal and tangential components of the temperature gradient being continuous, it means that the total gradient is continuous across the interface. The continuity of the temperature gradient is then implicitly satisfied if the continuities of the temperature and normal flux are satisfied.

Let us defined by $\boldsymbol{q}(\boldsymbol{x})$ and $\boldsymbol{q}'(\boldsymbol{x})$ the gradient of $v(\boldsymbol{x})$ and $v'(\boldsymbol{x})$ respectively:

$$\boldsymbol{q}(\boldsymbol{x}) = \nabla v(\boldsymbol{x}),\ \forall \boldsymbol{x} \in \Omega, \quad \boldsymbol{q}'(\boldsymbol{x}) = \nabla v'(\boldsymbol{x}),\ \forall \boldsymbol{x} \in \Omega' \tag{10}$$

Applying the classic chain rule, one has $\nabla[v(\boldsymbol{S}.\boldsymbol{x})] = \boldsymbol{S}.\nabla v(\boldsymbol{S}.\boldsymbol{x})$ and then $\boldsymbol{q}(\boldsymbol{x})$ and $\boldsymbol{q}'(\boldsymbol{x})$ are related by:

$$\boldsymbol{q}'(\boldsymbol{x}) = s_1 s_2 s_3 \boldsymbol{S}.\boldsymbol{q}(\boldsymbol{S}.\boldsymbol{x}),\ \forall \boldsymbol{x} \in \Omega' \tag{11}$$

### 3.3. Flux and thermal equilibrium

Denoting by $\boldsymbol{\sigma}(\boldsymbol{x})$ the flux in the initial cell $\Omega$, we introduce $\boldsymbol{\sigma}'(\boldsymbol{x})$ such that:

$$\boldsymbol{\sigma}'(\boldsymbol{x}) = \boldsymbol{T}.\boldsymbol{\sigma}(\boldsymbol{S}.\boldsymbol{x}),\ \forall \boldsymbol{x} \in \Omega' \tag{12}$$

where the two order tensor $\boldsymbol{T}$ is defined by:

$$\boldsymbol{T} = s_1 s_2 s_3 \boldsymbol{S} = \begin{pmatrix} s_2 s_3 & 0 & 0 \\ 0 & s_1 s_3 & 0 \\ 0 & 0 & s_1 s_2 \end{pmatrix} \tag{13}$$

This field is divergence free in $\Omega' - \mathcal{I}$ where $\mathcal{I}$ represents the interfaces between the individual cells. This distinction is needed because the components of $\boldsymbol{S}$ are constant in each individual cell but are discontinuous at the interfaces between the individual cells (the equilibrium of the normal flux at the interface between the individual cells is examined below). The proof for the divergence free condition is easy, indeed, considering Eq. (12) and applying the chain rule, one has $\forall \boldsymbol{x} \in \Omega' - \mathcal{I}$:

$$\operatorname{div}(\boldsymbol{T}.\boldsymbol{\sigma}(\boldsymbol{S}.\boldsymbol{x})) = \boldsymbol{T} : [\nabla \boldsymbol{\sigma}(\boldsymbol{S}.\boldsymbol{x}).\boldsymbol{S}] \tag{14}$$

Moreover, $\boldsymbol{T}.\boldsymbol{S} = s_1 s_2 s_3 \boldsymbol{I}$, then $\forall \boldsymbol{x} \in \Omega' - \mathcal{I}$:

$$\operatorname{div}(\boldsymbol{T}.\boldsymbol{\sigma}(\boldsymbol{S}.\boldsymbol{x})) = s_1 s_2 s_3 \boldsymbol{I} : [\nabla \boldsymbol{\sigma}(\boldsymbol{S}.\boldsymbol{x})] = s_1 s_2 s_3 \operatorname{div}(\boldsymbol{\sigma})(\boldsymbol{S}.\boldsymbol{x}) \tag{15}$$

Then if $\boldsymbol{\sigma}(\boldsymbol{x})$ is divergence free, $\boldsymbol{\sigma}'(\boldsymbol{x})$ is also divergence free in each individual cells. The flux $\boldsymbol{\sigma}'(\boldsymbol{x})$ is in equilibrium in all the domain $\Omega'$ if the normal flux is continuous across the interfaces between the individual cells. Otherwise, this would imply some line sources at the junction between individual cells, and would increase the difficulty when solving the problem with the FFT method.

We consider, for example, the interface corresponding to $x_1 = 0$. We aim to verify that $\sigma'_1(0, x_2, x_3)$ admits the same limit at the right and left on the considered interface. $\boldsymbol{T}$ is diagonal, then, accordingly to Eq. (12), $\sigma'_{11}(0, x_2, x_3) = T_{11}\sigma_{11}(0, s_2 x_2, s_3 x_3)$. Moreover the component $T_{11}$ is independent of $s_1$ and then $\sigma'_{11}$ is then also independent of $s_1$ that ensures its continuity across the interface $x_1 = 0$. The proof is the same for the continuity of components $\sigma'_{22}$ and $\sigma'_{33}$ across the interfaces $x_2 = 0$ and $x_3 = 0$.

For completeness, one has to verify the antiperiodicity conditions. Consider for examples the opposite edges corresponding to $x_1 = \pm L_1$ that can be also written $x_1 = s_1 L_1$. The demonstration is very similar, one has to prove that $\sigma'_{11}$ takes the same value on these opposite edges. One has, accordingly to Eq. (12), $\sigma'_1(s_1 L_1, x_2, x_3) = T_{11}\sigma_1(L_1, s_2 x_2, s_3 x_3)$ that is independent of $s_1$, proving the antiperiodicity for the two opposite edges $x_1 = \pm L_1$. The proof for the other opposite edges is similar. Finally, it has been shown that $\boldsymbol{\sigma}'$ is in equilibrium over $\Omega'$ and is $\Omega'$-antiperiodic.

### 3.4. Thermal relationship

We now establish the relation between the gradient of temperature $\boldsymbol{q}'(\boldsymbol{x})$ and the flux $\boldsymbol{\sigma}'(\boldsymbol{x})$ in all the domain $\Omega'$. In $\Omega$ the flux $\boldsymbol{\sigma}$ and the temperature gradient $\boldsymbol{q}(\boldsymbol{x})$ are related by the affine relation:

$$\boldsymbol{\sigma}(\boldsymbol{x}) = \boldsymbol{K}(\boldsymbol{x}).[\boldsymbol{q}(\boldsymbol{x}) + \boldsymbol{E}] \tag{16}$$

It follows that, considering Eq. (12):

$$\boldsymbol{\sigma}'(\boldsymbol{x}) = s_1 s_2 s_3 \boldsymbol{S}.[\boldsymbol{K}(\boldsymbol{S}.\boldsymbol{x}).(\boldsymbol{q}(\boldsymbol{S}.\boldsymbol{x}) + \boldsymbol{E})] \tag{17}$$

Moreover, owing to Eq. (11), we deduce that $\boldsymbol{q}(\boldsymbol{S}.\boldsymbol{x}) = s_1 s_2 s_3 \boldsymbol{S}.\boldsymbol{q}'(\boldsymbol{x})$ and:

$$\boldsymbol{\sigma}'(\boldsymbol{x}) = \boldsymbol{S}.\boldsymbol{K}(\boldsymbol{S}.\boldsymbol{x}).\boldsymbol{S}.\boldsymbol{q}'(\boldsymbol{x}) + s_1 s_2 s_3 \boldsymbol{S}.\boldsymbol{K}(\boldsymbol{S}.\boldsymbol{x}).\boldsymbol{E} \tag{18}$$

Finally, because $\boldsymbol{S}.\boldsymbol{S} = \boldsymbol{I}$, one can also read:

$$\boldsymbol{\sigma}'(\boldsymbol{x}) = \boldsymbol{K}'(\boldsymbol{x}).[\boldsymbol{q}'(\boldsymbol{x}) + \boldsymbol{E}'(\boldsymbol{x})] \tag{19}$$

where:

- $\boldsymbol{K}'(\boldsymbol{x})$ is given by:

  $$\boldsymbol{K}'(\boldsymbol{x}) = \boldsymbol{S}.\boldsymbol{K}(\boldsymbol{S}.\boldsymbol{x}).\boldsymbol{S} \tag{20}$$

  It must be noticed that $\boldsymbol{K}'(\boldsymbol{x})$ remains strictly positive definite by the transformation if $\boldsymbol{K}(\boldsymbol{x})$ is also positive definite. Also, if both constituents are isotropic, $\boldsymbol{K}(\boldsymbol{x}) = k(\boldsymbol{x})\boldsymbol{I}$, then $\boldsymbol{K}'(\boldsymbol{x})$ is also isotropic and $\boldsymbol{K}'(\boldsymbol{x}) = k(\boldsymbol{S}.\boldsymbol{x})\boldsymbol{I}$. When the constituents are anisotropic, the components of $\boldsymbol{K}'(\boldsymbol{x})$ in the cartesian frame are $K'_{ij}(\boldsymbol{x}) = s_i s_j K_{ij}(\boldsymbol{S}.\boldsymbol{x})$ (here the Einstein convention on repeated indices must not be applied). It follows that the diagonal components of $\boldsymbol{K}'(\boldsymbol{x})$ remain unchanged by the transformation, $K'_{ii}(\boldsymbol{x}) = K_{ii}(\boldsymbol{S}.\boldsymbol{x})$, while the off-diagonal components must be either positive or negative depending of the considered individual unit cell.
- The loading parameter $\boldsymbol{E}'(\boldsymbol{x})$ is given by:

  $$\boldsymbol{E}'(\boldsymbol{x}) = s_1 s_2 s_3 \boldsymbol{S}.\boldsymbol{E} \tag{21}$$

  This loading parameter is consistent with:

  $$s_1 s_2 s_3 \boldsymbol{S}.\boldsymbol{K}(\boldsymbol{S}.\boldsymbol{x}).\boldsymbol{E} = \boldsymbol{K}'(\boldsymbol{x}).\boldsymbol{E}'(\boldsymbol{x}) \tag{22}$$

To conclude, $v'$ satisfies the equations related to a conductivity problem over $\Omega'$ with the conductivity tensor $\boldsymbol{K}'(\boldsymbol{x})$ under the applied periodic eigenfield $\boldsymbol{E}'(\boldsymbol{x})$. The resulting problem which has to be solved is remarkable by its simplicity, particularly in the isotropic case, since it only involves the resolution with the applied piecewise constant loading function $\boldsymbol{E}'(\boldsymbol{x})$ instead of the constant loading $\boldsymbol{E}$ in the classic periodic problem. As a consequence, a classic FFT based iterative schemes can be used to solve that problem with very minor modification. The values of $\boldsymbol{E}'(\boldsymbol{x})$ taken in the period $\Omega'$ is illustrated in Fig. 3 for 2D problems. At the left, we provide the components $E'_1(\boldsymbol{x})$ and, at the right, the component $E'_2(\boldsymbol{x})$. The period $\Omega'$ is constituted of four quarters corresponding to the original unit cell $\Omega$ and its mirrors images. The component $E'_1(\boldsymbol{x})$ is equal to $E_1$ for the upper quarters and equal to $-E_1$ for the lower quarters. The component $E'_2(\boldsymbol{x})$ is equal to $E_2$ for the right quarters and equal to $-E_2$ for the left quarters.

### 3.5. Effective conductivity

The identification of the macroscopic conductivity must be done considering the Hill–Mandel Lemma. The macroscopic potential is:

$$W = \langle \boldsymbol{\sigma}'(\boldsymbol{x}).(\boldsymbol{q}'(\boldsymbol{x}) + \boldsymbol{E}'(\boldsymbol{x})) \rangle_{\Omega'} = \langle s_1 s_2 s_3 \boldsymbol{S}.\boldsymbol{\sigma}'(\boldsymbol{x}) \rangle_{\Omega'}.\boldsymbol{E} \tag{23}$$

In the above equation, the average of the scalar product between $\boldsymbol{\sigma}'(\boldsymbol{x})$ and $\boldsymbol{q}'(\boldsymbol{x})$ vanishes since $\boldsymbol{\sigma}'(\boldsymbol{x}).\boldsymbol{n}$ is antiperiodic and $\boldsymbol{q}'(\boldsymbol{x})$ derivates from the periodic temperature field $v'(\boldsymbol{x})$. Due to the symmetry, one has also:

$$W = \langle \boldsymbol{\sigma}(\boldsymbol{x}).(\boldsymbol{q}(\boldsymbol{x}) + \boldsymbol{E}) \rangle_{\Omega} = \boldsymbol{\Sigma}.\boldsymbol{E} \tag{24}$$

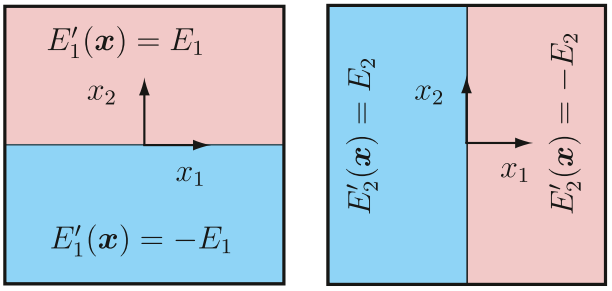


**Fig. 3.** Values of components of $\boldsymbol{E}'(\boldsymbol{x})$ taken in the unit cell $\Omega'$ for the $2D$ case.

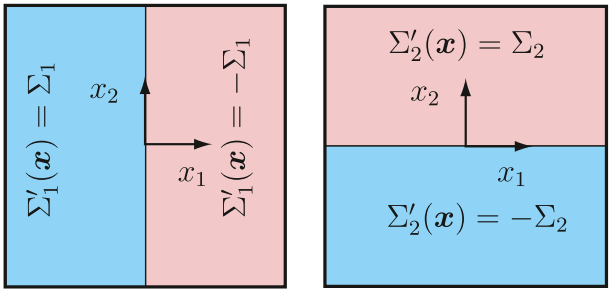


**Fig. 4.** Values of $\boldsymbol{\Sigma}'(\boldsymbol{x})$ taken in the unit cell $\Omega'$.

In virtue of the Hill–Mandell Lemma, we deduce from Eq. (24) together with Eq. (23) that the macroscopic flux is given by:

$$\boldsymbol{\Sigma} = \langle s_1 s_2 s_3 \boldsymbol{S}.\boldsymbol{\sigma}'(\boldsymbol{x})\rangle_{\Omega'} \tag{25}$$

Once the flux is computed in $\Omega'$, the macroscopic flux is derived from (25) allowing the computation of the components of the effective conductivity related to the Dirichlet problem.

The resolution of the Dirichlet problem over the extended domain $\Omega'$, can be solved considering classic FFT iterative schemes that are adapted in order to apply the loading field $\boldsymbol{E}'(\boldsymbol{x})$. The details are provided in Appendix.

## 4. Neumann problem

### 4.1. Compatibility

Consider the temperature field $u(\boldsymbol{x})$ solution of the Neumann problem and let us introduce $u'(\boldsymbol{x})$ such that:

$$u'(\boldsymbol{x}) = u(\boldsymbol{S}.\boldsymbol{x}), \quad \forall \boldsymbol{x} \in \Omega' \tag{26}$$

The temperature field $u'(\boldsymbol{x})$ is continuous across the interfaces between individual cells. We denote the temperature gradient in $\Omega$ by $\boldsymbol{\epsilon}$ and the temperature gradient in $\Omega'$ by $\boldsymbol{\epsilon}'$:

$$\boldsymbol{\epsilon}(\boldsymbol{x}) = \nabla u(\boldsymbol{x}), \ \forall \boldsymbol{x} \in \Omega, \quad \boldsymbol{\epsilon}'(\boldsymbol{x}) = \nabla u'(\boldsymbol{x}), \ \forall \boldsymbol{x} \in \Omega' \tag{27}$$

By applying the chain rule, one can obtain the following relation between $\boldsymbol{\epsilon}(\boldsymbol{x})$ and $\boldsymbol{\epsilon}'(\boldsymbol{x})$:

$$\boldsymbol{\epsilon}'(\boldsymbol{x}) = \boldsymbol{S}.\boldsymbol{\epsilon}(\boldsymbol{S}.\boldsymbol{x}), \quad \forall \boldsymbol{x} \in \Omega' \tag{28}$$

### 4.2. Equilibrium

The flux related to this problem is divergence-free and satisfies the Neumann condition $\boldsymbol{\sigma}.\boldsymbol{n} = \boldsymbol{\Sigma}.\boldsymbol{n}$ at the boundary of the unit cell $\Omega$. Let us decompose $\boldsymbol{\sigma}$ as follows: $\boldsymbol{\sigma} = \boldsymbol{\Sigma} + \boldsymbol{p}$ where $\boldsymbol{p}$ is divergence-free and satisfies to the Neumann condition $\boldsymbol{p}.\boldsymbol{n} = 0$ at the boundary of the unit cell $\Omega$. Let us introduce $\boldsymbol{p}'$ the vector field over the extended domain $\Omega'$ such that:

$$\boldsymbol{p}'(\boldsymbol{x}) = \boldsymbol{S}.\boldsymbol{p}(\boldsymbol{S}.\boldsymbol{x}), \quad \forall \boldsymbol{x} \in \Omega' \tag{29}$$

$\boldsymbol{p}'(\boldsymbol{x})$ is also divergence-free. Indeed, applying the divergence to $\boldsymbol{p}'(\boldsymbol{x})$ taking into account Eq. (31) yields:

$$\mathrm{div}(\boldsymbol{p}'(\boldsymbol{x})) = \mathrm{div}(\boldsymbol{S}.\boldsymbol{p}(\boldsymbol{S}.\boldsymbol{x})) = \boldsymbol{S} : [\nabla \boldsymbol{p}(\boldsymbol{S}.\boldsymbol{x}).\boldsymbol{S}], \quad \forall \boldsymbol{x} \in \Omega' \tag{30}$$

Because $\boldsymbol{S}.\boldsymbol{S} = \boldsymbol{I}$, it follows that:

$$\mathrm{div}(\boldsymbol{p}'(\boldsymbol{x})) = \mathrm{div}(\boldsymbol{p})(\boldsymbol{S}.\boldsymbol{x}), \quad \forall \boldsymbol{x} \in \Omega' - \mathcal{I} \tag{31}$$

Then, $\boldsymbol{p}'(\boldsymbol{x})$ is divergence-free if $\boldsymbol{p}$ is also divergence-free. Again, the interface between individual cells, $\mathcal{I}$, has been excluded because $\boldsymbol{S}$ is not differentiable. However, since $\boldsymbol{p}.\boldsymbol{n} = 0$ at the interfaces $\mathcal{I}$, $\boldsymbol{p}'(\boldsymbol{x}).\boldsymbol{n}$ is also null, and then the equilibrium is fulfilled at the interfaces $\mathcal{I}$ as well. Moreover, since $\boldsymbol{p}.\boldsymbol{n} = 0$ at the boundary of $\Omega$, $\boldsymbol{p}'(\boldsymbol{x}).\boldsymbol{n}$ is also null on the boundary of $\Omega'$ and is then anti-periodic.

### 4.3. Thermal relationships

The conductivity law in $\Omega$ is:

$$\boldsymbol{\epsilon}(\boldsymbol{x}) = \boldsymbol{H}(\boldsymbol{x}).[\boldsymbol{p}(\boldsymbol{x}) + \boldsymbol{\Sigma}], \quad \forall \boldsymbol{x} \in \Omega \tag{32}$$

where $\boldsymbol{H}(\boldsymbol{x})$ is resistivity tensor, the inverse of the conductivity tensor $\boldsymbol{K}(\boldsymbol{x})$. Replacing $\boldsymbol{x}$ by $\boldsymbol{S}.\boldsymbol{x}$ and owing to Eq. (31) together with Eq. (28), one obtains:

$$\boldsymbol{\epsilon}'(\boldsymbol{x}) = \boldsymbol{S}.\boldsymbol{H}(\boldsymbol{S}.\boldsymbol{x}).[\boldsymbol{S}.\boldsymbol{p}'(\boldsymbol{x}) + \boldsymbol{\Sigma}], \quad \forall \boldsymbol{x} \in \Omega' \tag{33}$$

Because $\boldsymbol{S}.\boldsymbol{S} = \boldsymbol{I}$, the above relation can be also read:

$$\boldsymbol{\epsilon}'(\boldsymbol{x}) = \boldsymbol{H}'(\boldsymbol{x}).[\boldsymbol{p}'(\boldsymbol{x}) + \boldsymbol{\Sigma}'(\boldsymbol{x})], \quad \forall \boldsymbol{x} \in \Omega' \tag{34}$$

with the following definitions for $\boldsymbol{H}'(\boldsymbol{x})$ and $\boldsymbol{\Sigma}'(\boldsymbol{x})$:

$$\boldsymbol{H}'(\boldsymbol{x}) = \boldsymbol{S}.\boldsymbol{H}(\boldsymbol{S}.\boldsymbol{x}).\boldsymbol{S}, \quad \boldsymbol{\Sigma}'(\boldsymbol{x}) = \boldsymbol{S}.\boldsymbol{\Sigma} \tag{35}$$

As a conclusion, $\boldsymbol{u}'(\boldsymbol{x})$ is the solution of a conductivity problem over $\Omega'$ with the resistivity tensor $\boldsymbol{H}'(\boldsymbol{x})$ and the prescribed eigenfield $\boldsymbol{\Sigma}'(\boldsymbol{x})$. Note that $\boldsymbol{H}'(\boldsymbol{x}) = (\boldsymbol{K}'(\boldsymbol{x}))^{-1}$ where $\boldsymbol{K}'(\boldsymbol{x})$ is the conductivity introduced in the Dirichlet problem (see Eq. (20)). The eigenfield $\boldsymbol{\Sigma}'(\boldsymbol{x})$ is a piecewise constant function. The value taken by $\boldsymbol{\Sigma}'(\boldsymbol{x})$ in $\Omega'$ is illustrated in the 2D case in Fig. 4.

### 4.4. Homogenized conductivity

In virtue of the Hill–Mandell Lemma, the macroscopic temperature gradient is given by (the proof is very similar to that already given in Section 3.5):

$$\boldsymbol{E} = \langle \boldsymbol{S}.\boldsymbol{\epsilon}'(\boldsymbol{x})\rangle_{\Omega'} \tag{36}$$

The Neumann problem can be solved with the classic FFT iterative schemes adapted to account for the loading field $\boldsymbol{\Sigma}'(\boldsymbol{x})$, the details are provided in Appendix.

## 5. Applications

As an application purpose, we consider a composite conductor made up of circular inclusions. The conductivity of the matrix and the inclusions are denoted $k_1$ and $k_2$ respectively. Three unit cells are considered for the calculations and are illustrated in Fig. 5. The first line (cells (a), (b) and (c)) correspond to the original cells on which the Dirichlet or Neumann boundary conditions are applied. The second line correspond to the extended cells obtain by the reflexion with respect to the axes $Ox_1$ and $Ox_2$ over which the periodic boundary conditions and the applied loading field $\boldsymbol{E}'(\boldsymbol{x})$ (for the Dirichlet condition) or $\boldsymbol{\Sigma}'(\boldsymbol{x})$ (for the Neumann condition). Also, for comparison, we also compute the classic periodic solution under the applied uniform temperature gradient $\boldsymbol{E}$ to the cells (a), (b) and (c). Our results are also compared with FE solutions to validate the approach considering the periodic, Dirichlet and Neumann conditions to the unit cell (a), (b) and (c).

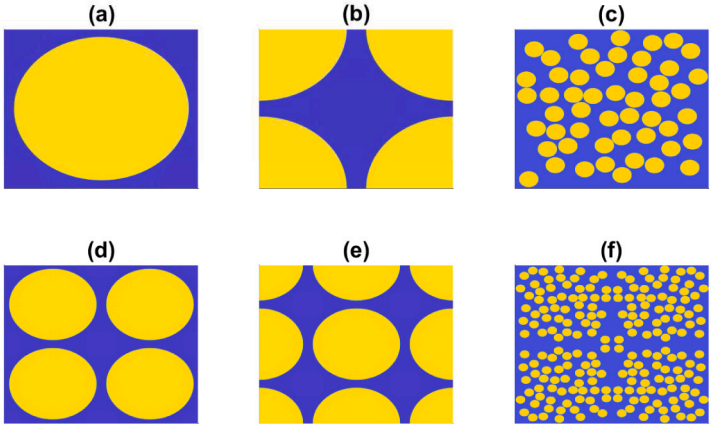


**Fig. 5.** Unit cells of the composite conductor.

The unit cell (a) corresponds to a single centered circular inclusion of radius $R = 0.45$ (the size of the inclusion is 1 along each space direction). The value $R = 0.45$ of the inclusion radius is chosen to exhibit better the difference between the different kinds of boundary conditions. Indeed, with a smaller value of the radius, the effective conductivities obtained with the three boundary conditions become much closer to each other. The unit cell (b) is constituted of four quarters of a single circular inclusion of radius $R = 0.45$. Note that unit cells (a) and (b) lead to the same value of the effective conductivity when the periodic boundary conditions are considered but are not equivalent for the Dirichlet and Neumann conditions. The unit cell (c) contains a population of 51 inclusions with the same radius $R = 0.05$ (the size of the unit cell is still equal to 1).

Note that the exact expressions of Fourier coefficients of the loading parameter $\boldsymbol{E}'(\boldsymbol{x})$ and $\boldsymbol{\Sigma}'(\boldsymbol{x})$ are considered. For instance, the Fourier transform of $\boldsymbol{E}'(\boldsymbol{x})$ is:

$$\widehat{\boldsymbol{E}}'(\boldsymbol{\xi}) = \frac{1}{|\Omega'|}\int_{\Omega'} \boldsymbol{E}'(\boldsymbol{x})\exp(-i\boldsymbol{\xi}.\boldsymbol{x})dx_1dx_2 \tag{37}$$

The field $\boldsymbol{E}'(\boldsymbol{x})$ being a piecewise constant function in $\Omega'$, the integration is trivial and leads to:

$$\begin{aligned}
&\widehat{\boldsymbol{E}}'(\boldsymbol{\xi}) = \begin{pmatrix} \widehat{s}_2(\boldsymbol{\xi})E_1 \\ \widehat{s}_1(\boldsymbol{\xi})E_2 \end{pmatrix},\\
&\widehat{s}_1(\boldsymbol{\xi}) = -i\,\mathrm{sinc}(L_2\xi_2)\,\mathrm{sinc}\left(\frac{L_1\xi_1}{2}\right)\sin\left(L_1\xi_1\right),\\
&\widehat{s}_2(\boldsymbol{\xi}) = -i\,\mathrm{sinc}(L_1\xi_1)\,\mathrm{sinc}\left(\frac{L_2\xi_2}{2}\right)\sin\left(L_2\xi_2\right)
\end{aligned} \tag{38}$$

The Fourier coefficients of the components of $\boldsymbol{\Sigma}'(\boldsymbol{x})$ are:

$$\widehat{\boldsymbol{\Sigma}}'(\boldsymbol{\xi}) = \begin{pmatrix} \widehat{s}_1(\boldsymbol{\xi})\Sigma_1 \\ \widehat{s}_2(\boldsymbol{\xi})\Sigma_2 \end{pmatrix} \tag{39}$$

The two fields $\boldsymbol{E}'$ and $\boldsymbol{\Sigma}'$ are piecewise constant over a set of rectangular domains. The characteristic functions of these domains can be defined either in real space or in Fourier space, leading to two different expressions of $\boldsymbol{E}'$ and $\boldsymbol{\Sigma}'$. Obviously, the transition from one space to the other is easily achieved using the FFT. Both calculations are rigorously identical when considering an infinite number of wave vectors. When taking a finite number of wave vectors, this leads to differences due to the discretization and the truncature approximation.

We first provide the results corresponding to a single centered inclusion (cells (a) and (d) in Fig. 5). The convergence of the effective conductivity with the number of wave vectors is presented in Fig. 6. The effective conductivity is computed with $N = 32, 64, 128, 256, 512$ wave vectors along each space direction considering the primal, dual and polarization based iterative schemes for Dirichlet condition (at the right), the Neumann condition (at the left), a phase contrast $k_2/k_1$ of 100 at the top and 0.01 at the bottom.

In the case of a high contrast, $k_2/k_1 = 100$, the dual and polarization iterative schemes have a better convergence with the grid refinement than the primal iterative scheme based on the temperature gradient. This is observed for both the Dirichlet and Neumann boundary conditions. Conversely, regarding the results in the case of a small contrast, $k_2/k_1 = 0.01$, a better convergence with the grid refinement is observed with the primal iterative scheme and the polarization. To conclude the results for the single centered inclusion, the polarization method has a better convergence with the grid refinement whatever the value of contrast.

Interestingly, we have extrapolated the value of the effective conductivity to estimate its value for any value of the number of wave vectors $N$ taken along each spatial direction, i.e., the resolution of the image. Assuming that the dependence of $K^{hom}$ on the resolution $N$ follows the form of a power series:

$$K^{hom}(N) = k_1\sum_{j=1}^{J}\frac{A_j}{N^{j-1}} \tag{40}$$

In order to determine the coefficient $A_j$ for $j = 1, \dots, J$, it is necessary to assume that $K^{hom}(N)$ is known for a finite number of $N$ values, denoted $N_1, N_2, \dots, N_J$ such that $N_1 < N_2 < \cdots < N_J$. The coefficients $A_1, \dots, A_J$ can then be identified by solving the following linear system:

$$k_1\begin{pmatrix} 1 & \frac{1}{N_1} & \dots & \frac{1}{N_1^{J-1}} \\ 1 & \frac{1}{N_1} & \dots & \frac{1}{N_1^{J-1}} \\ \vdots & & & \\ 1 & \frac{1}{N_J} & \dots & \frac{1}{N_J^{J-1}} \end{pmatrix}\begin{pmatrix} A_1 \\ A_2 \\ \vdots \\ A_J \end{pmatrix} = \begin{pmatrix} K^{hom}(N_1) \\ K^{hom}(N_2) \\ \vdots \\ K^{hom}(N_J) \end{pmatrix} \tag{41}$$

The effective conductivity $K^{hom}(N_j)$ is computed for resolutions $N_1, N_2, \dots, N_J$, where $j = 1, \dots, J$. In the present study, $K^{hom}$ is computed for five different resolutions, namely $32, 64, 128, 256, 512$. The extrapolated function $K^{hom}(N)$ is shown in Fig. 6 for the three iterative schemes. The solid line represents the extrapolated function, while the crosses correspond to the discrete values of $K^{hom}$ computed for the different resolutions. It is worth noting that the extrapolated function provides an estimate of the conductivity for an infinite resolution ($N = +\infty$), which corresponds to $k_1A_1$. Remarkably, the limits computed by the three iterative schemes converge to very close values as the resolution tends to infinity, allowing for a reliable estimation of the theoretical value of $K^{hom}$ for both kinds of boundary conditions.

In Fig. 7, we represent the effective conductivities corresponding to the Dirichlet and Neumann problem as functions of the phase contrast $k_2/k_1$ for the single centered inclusion at the left (unit cells (a) and (d)), and the population of inclusion at the right (unit cells (c) and (f)). As a validation purpose, the results obtained with the FFT are compared

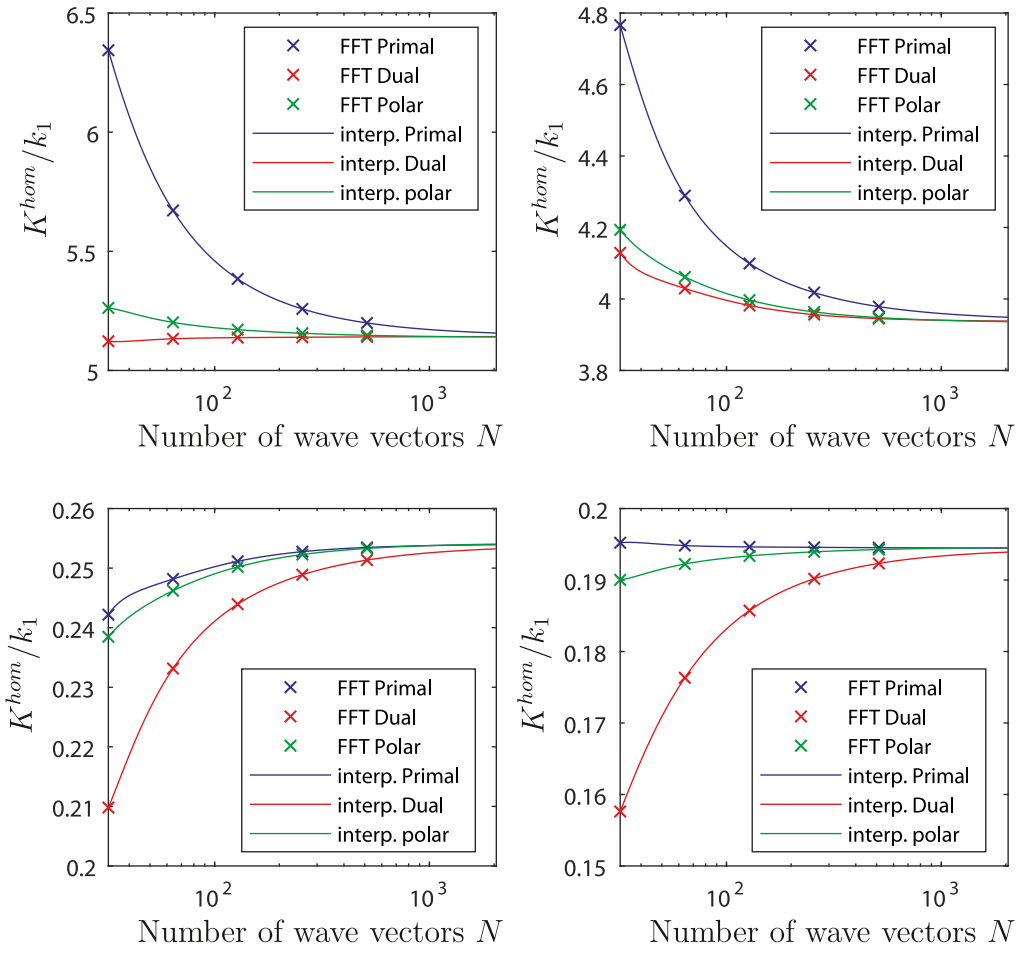


**Fig. 6.** Variations of the effective conductivity as a function of the number of wave vectors for one single centered circular inclusion. Figures at the top: problem with Dirichlet condition (at the right) or Neumann boundary condition (at the left) for $k_2/k_1 = 100$. Figures at the bottom: the same boundary conditions but for a contrast $k_2/k_1 = 0.01$.

with those computed with the FEM for which a good accuracy is observed. As expected, it is noticed that the solution derived with the periodic boundary and the applied uniform temperature gradient $\boldsymbol{E}$ (classic periodic solution) is bounded by the two other ones corresponding to Dirichlet and Neumann conditions.

The monotonicity of the estimated effective conductivity is observed only when the FFT method uses the shape function, i.e. the exact Fourier transform of the characteristic function of the phase. The method based on the shape function is explained in the work of Bonnet (2007). The advantage is to describe exactly the microstructure geometry while in the original method of Moulinec and Suquet (1994, 1998), the unit cell is discretized with pixels that correspond to the inexactly integrated FFT methods pointed out by Monchiet (2015) and Vondřejc (2016). However, the use of shape function is only restricted to some particular geometries for which it is possible to derive the exact Fourier transform of the characteristic function, the different problems for which the shape function can be used has been depicted in the recent work of Nguyen et al. (2021).

We now provide the solution with the unit cells containing four quarters of circular inclusion (unit cells (b) and (e) in Fig. 8). The effective conductivity is provided as a function of the phase contrast varying from $10^{-3}$ to $10^3$ for the three kinds of boundary conditions and considering the FFT and FE methods. It can be observed that the effective conductivity computed with the Dirichlet boundary conditions diverges for highly conductive inclusions. Such result has already been observed by Salmi et al. (2012) for instance. When the conductivity $k_2$ is very large, we observe that the flux remains finite in the inclusions that do not intersect the edge, so that the temperature gradient is close to zero. At the limit, for infinitely conductive inclusions, the temperature gradient in these inclusions therefore tends towards zero. However, for the inclusions that intersect the edge of the cell, the temperature gradient cannot be zero as a consequence of the Dirichlet condition, which imposes $u = \boldsymbol{E}.\boldsymbol{x}$, on the boundary of the cell. Consequently, this implies a " blow-up" of the flux in these inclusions, as mentioned in the work of Salmi et al. (2012), that leads to the divergence of the effective conductivity. Dually, i.e. for highly resistive inclusions and the Neumann condition at the edge, we observe a blow-up of the temperature gradient in the inclusions that intersect the edge of the cell. As a consequence, the effective conductivity tends to zero (divergence of the effective resistivity) in the case of highly resistive inclusions when the Neumann boundary condition is used.

The distribution of the temperature gradient $\epsilon_1'$ and the flux $\sigma_1'$ corresponding to the Dirichlet problem (with $E_1 = 1$ and $E_2 = 0$) and the Neumann problem (with $\Sigma_1 = 1$ and $\Sigma_2 = 0$) are provided in Fig. 9. The phase contrast is $k_2/k_1 = 1000$. It is observed, for the Dirichlet problem, that the flux in the inclusions is of the same magnitude as the contrast: this explains the divergence of the effective conductivity for highly conductive inclusions.

In Fig. 10 another microstructure is tested to support our conclusion. At the left, we show a unit cell $\Omega'$ obtained by the mirror symmetry of the original cell $\Omega$ corresponding to a population of inclusions for which some of them cross the boundary. At the right, we provide the distribution of $\epsilon_1'$ applying the Dirichlet condition with $E_1 = 1$, $E_2 = 0$ and we choose the contrast $k_2/k_1 = 100$. It is observed that the temperature gradient concentrates in the inclusions that cross the top and bottom edges of the individual cells and the amplitude is still of the

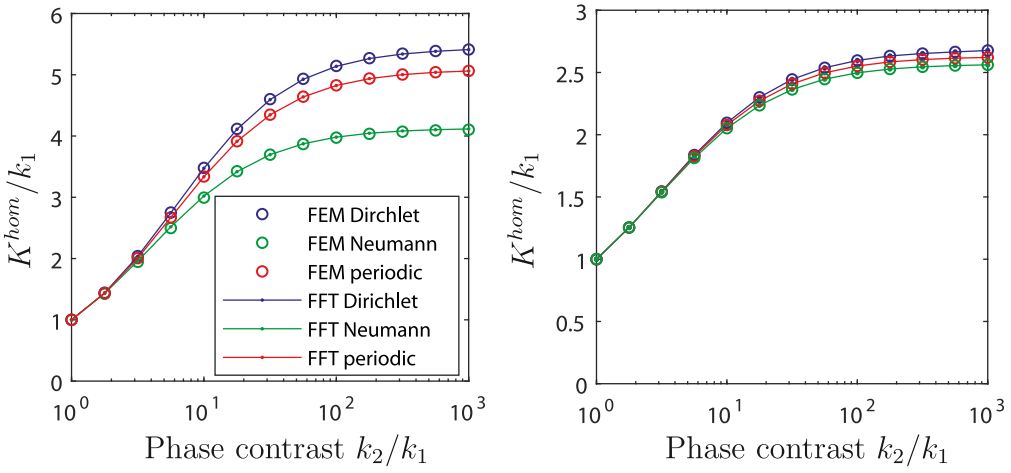


**Fig. 7.** Variations of the effective conductivity as a function of the phase contrast $k_2/k_1$. Comparisons between the FFT and FEM solutions for the three kinds of boundary conditions. At the left : one single centered inclusion (unit cell (a) in Fig. 5), at the right : a population of circular inclusions (unit cell (c) in Fig. 5).

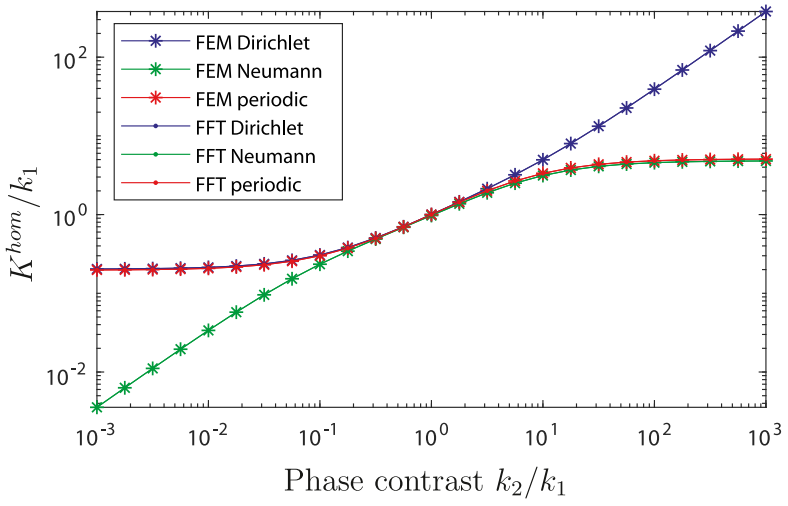


**Fig. 8.** Variations of the effective conductivity as function of the phase contrast $k_2/k_1$. Comparisons between the FFT and FEM solutions for the three kind of boundary conditions.

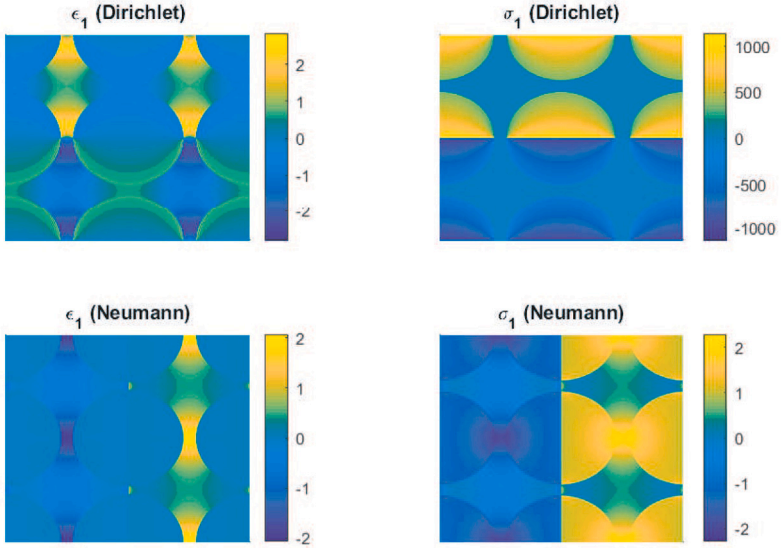


**Fig. 9.** Distribution of $\varepsilon_1'$ (at the left) and $\sigma_1'$ (at the right) for the Dirichlet problem (at the top) and the Neumann problem (at the bottom). Case of a contrast $k_2/k_1 = 100$.

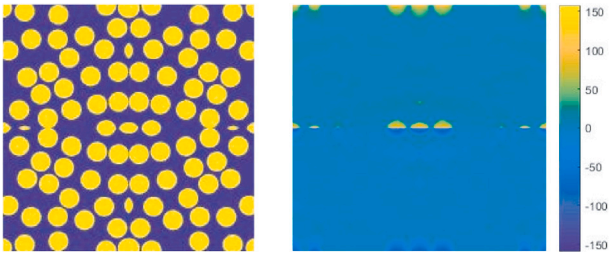


**Fig. 10.** Unit cell with a population of inclusions crossing the boundary (at the left). Distribution of $\varepsilon_1'$ (at the right) for the Dirichlet problem (with $E_1 = 1$ and $E_2 = 0$) and the contrast $k_2/k_1 = 100$.

**Table 1**
Homogenized conductivities of the anisotropic composite. Comparison of the primal, dual and polarization based solutions (at $N = +\infty$) and the FEM one.

| | Dirichlet | | | Neumann | | |
|---|---|---|---|---|---|---|
| | $K_{11}^{hom}$ | $K_{12}^{hom}$ | $K_{22}^{hom}$ | $K_{11}^{hom}$ | $K_{12}^{hom}$ | $K_{22}^{hom}$ |
| FFT primal | 4.4974 (0.080%) | 1.8904 (0.026%) | 4.0813 (0.010%) | 4.2808 (0.096%) | 1.8652 (0.016%) | 3.8221 (0.034%) |
| FFT dual | 4.4927 (0.024%) | 1.8893 (0.032%) | 4.0804 (0.012%) | 4.2860 (0.026%) | 1.8653 (0.011%) | 3.8190 (0.047%) |
| FFT polarization | 4.4932 (0.013%) | 1.8881 (0.095%) | 4.0820 (0.027%) | 4.2820 (0.068%) | 1.8656 (0.005%) | 3.8198 (0.026%) |

same magnitude as the contrast. Again, in that situation, the solution diverges for highly conductive inclusions. This problem is inherent with the use of the Dirichlet condition that is not suited when the unit cell boundary is crossed by the inclusion. When the Dirichlet condition is used, the unit cell must be chosen such that the inclusions do not cross the boundary or must be considered only if the contrast is inferior to 1. Also, the problem with Neumann condition must be applied to unit cell for which the inclusion do not cross the boundary or if the contrast is superior to 1.

Finally, we derive the homogenized conductivity for a composite with anisotropic phases. The problem under consideration corresponds to the unit cell (c) in Fig. 5. Random values for the conductivity in the matrix and the inclusions are used (but ensuring the positiveness of the conductivity tensor in each phase). The conductivity tensors (expressed in the cartesian frame) in $\Omega_1$ and $\Omega_2$ regions are:

$$\boldsymbol{K}^1 = \begin{pmatrix} 1.9134 & 1.1270 \\ 1.1270 & 1.6324 \end{pmatrix}, \quad \boldsymbol{K}^2 = \begin{pmatrix} 154.60 & 127.80 \\ 127.80 & 195.74 \end{pmatrix} \tag{42}$$

The variations of the conductivities $K_{11}^{hom}$, $K_{12}^{hom}$ and $K_{22}^{hom}$ with the grid refinement are provided in Figs. 11, 12, 13 for the Dirichlet and Neumann problems. The conductivities computed with the primal, dual and polarization based iterative schemes for $N = 32, 64, 128, 256, 512$ and the results are also extrapolated in order to evaluate the limit at $N \to +\infty$. Again, the interpolation with the different iterative schemes leads to very close values of the limit.

The results are summarized in Table 1. We provide the limit at $N = +\infty$ obtained for the three iterative schemes and for the two kind of boundary conditions. Also we compare our solutions with FE ones, the relative error is given under parenthesis in Table 1 FE solutions. The FE solutions are computed considering 123 260 triangular elements. The proposed FFT methods leads to very accurate values of the conductivities in the case of an anisotropic material.

## 6. Conclusion

FFT methods have been generalized to handle the problem of composite conductors with uniform boundary conditions. The resulting iterative schemes involve only minor modifications and existing codes are easily adapted to solve these homogenization problems. The computation is performed on an extended cell obtain by mirror symmetry that is easily built from the initial image of the microstructure. Moreover, these unit cells are loaded with a piecewise constant eigenfield for which simple analytic expressions are derived in the paper. The method has been illustrated for 2D microstructures with circular inclusions and the results have been compared with FEM with a good accuracy. The method could be extended for other problems such as elastic composites that would constitute future developments.

## Declaration of competing interest

All authors declare have no any financial and personal relationships with other people or organizations that could inappropriately influence their work.

## Data availability

No data was used for the research described in the article

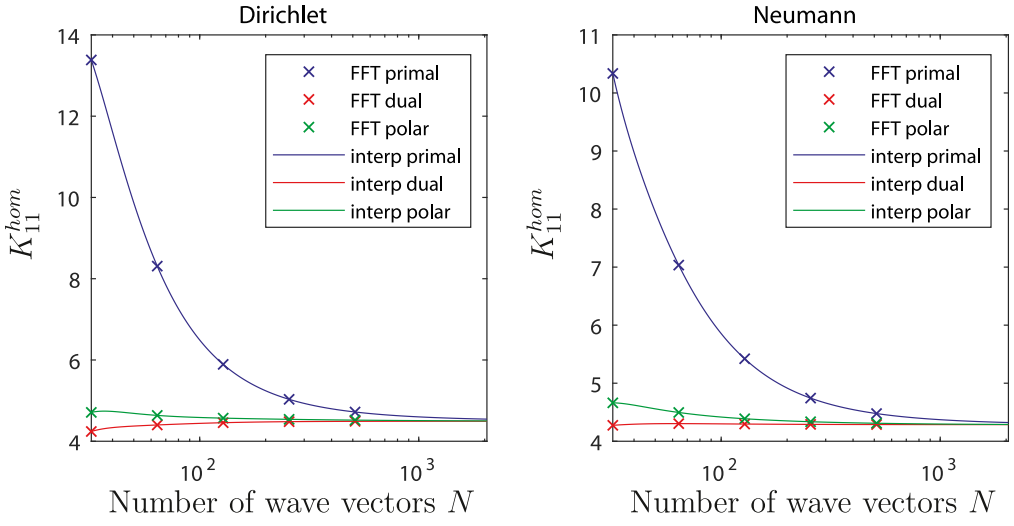


**Fig. 11.** Variations of the homogenized conductivity $K_{11}^{hom}$ as functions of the grid refinement for the Dirichlet problem (at the left) and the Neumann problem (at the right). Case of a composite with a population of inclusions and local anisotropic phases.

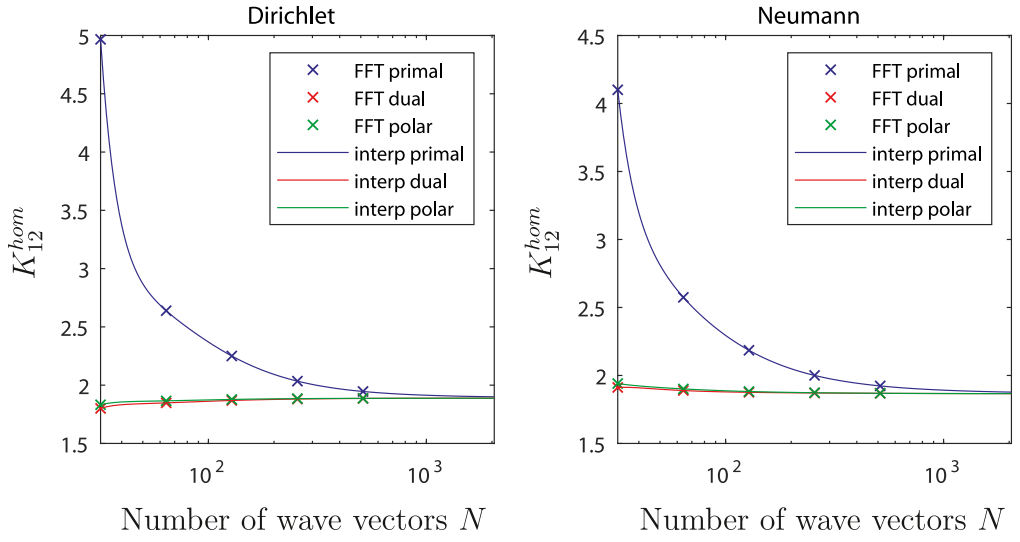


**Fig. 12.** Variations of the homogenized conductivity $K_{12}^{hom}$ as functions of the grid refinement for the Dirichlet problem (at the left) and the Neumann problem (at the right). Case of a composite with a population of inclusions and local anisotropic phases.

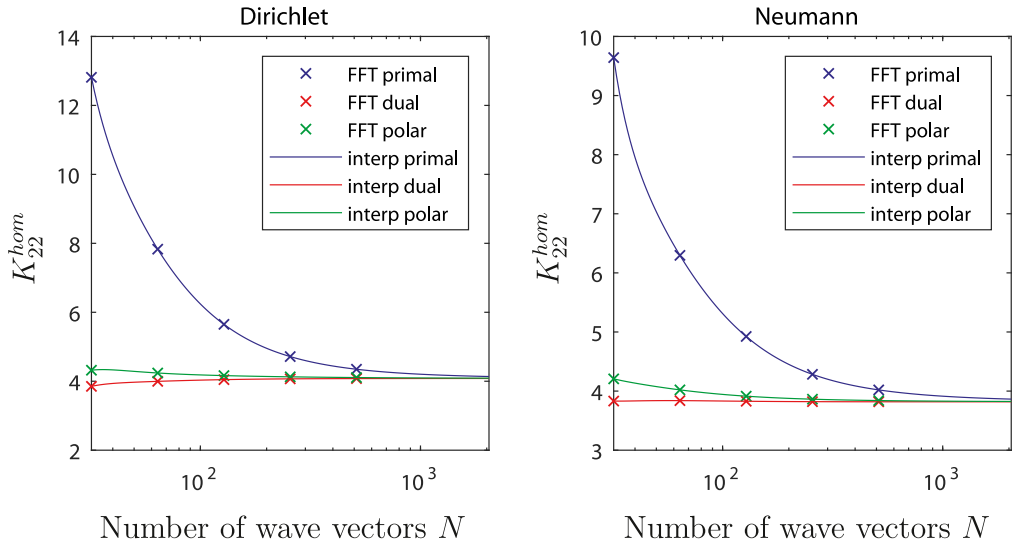


**Fig. 13.** Variations of the homogenized conductivity $K_{22}^{hom}$ as function of the grid refinement for the Dirichlet problem (at the left) and the Neumann problem (at the right). Case of an composite with a population of inclusions and local anisotropic phases.

## Appendix. Resolution with FFT algorithm

### A.1. Dirichlet problem

Consider the Dirichlet problem that involves the temperature gradient $\boldsymbol{q}'$ (the dependence of the fields with the coordinates $\boldsymbol{x}$ is omitted in this section for the sake of simplicity) whose volume average over the domain $\Omega'$ is null, $\langle \boldsymbol{q}' \rangle_{\Omega'} = 0$. The associated flux, $\boldsymbol{\sigma}' = \boldsymbol{K}'.(\boldsymbol{q}' + \boldsymbol{E}')$ is divergence free. Note that $\boldsymbol{E}'$ is a piecewise constant field whose volume average is also null, $\langle \boldsymbol{E}' \rangle_{\Omega'} = 0$. The flux being divergence free, it implies that it satisfies to:

$$\boldsymbol{\Gamma}^0 * \boldsymbol{\sigma}' = 0 \tag{A.1}$$

where $\boldsymbol{\Gamma}^0$ is the classic periodic Green tensor for the thermal conductivity problem (the reader can refer to Eyre and Milton (1999), Milton (2002) and Monchiet and Bonnet (2013) for the definition of the Green tensor) and "$*$" represent the convolution product. An iterative scheme associated with the Dirichlet problem can then be read:

$$\boldsymbol{q}'_{i+1} = \boldsymbol{q}'_i - \boldsymbol{\Gamma}^0 * \left[\boldsymbol{K}'.(\boldsymbol{q}'_i + \boldsymbol{E}')\right] \tag{A.2}$$

This iterative scheme is initialized with $\boldsymbol{q}'_1 = 0$. Note that it is possible to introduce $\boldsymbol{\varepsilon}'_i = \boldsymbol{q}'_i + \boldsymbol{E}'$ and to reformulate the iterative scheme as follows:

$$\boldsymbol{\varepsilon}'_{i+1} = \boldsymbol{\varepsilon}'_i - \boldsymbol{\Gamma}^0 * \left[\boldsymbol{K}'.\boldsymbol{\varepsilon}'_i\right] \tag{A.3}$$

In this second form, the iterative process is initialized with $\boldsymbol{\varepsilon}'_1 = \boldsymbol{E}'$. At convergence of the iterative scheme the macroscopic flux is computed from Eq. (25).

Many other alternative methods have been provided in the literature to improve the convergence of the method. For instance, a dual method based on the flux can be employed to solve the Dirichlet problem. The temperature gradient $\boldsymbol{q}'$ being curl free, it satisfies to:

$$\boldsymbol{A}^0 * \boldsymbol{q}' = 0 \tag{A.4}$$

where $\boldsymbol{A}^0$ is the dual Green tensor whose expression can be found in the same aforementioned references. Eq. (A.4) can be also expressed with

the flux:

$$\boldsymbol{\Delta}^0 * (\boldsymbol{H}'.\boldsymbol{\sigma}' - \boldsymbol{E}') = 0 \tag{A.5}$$

The following iterative process can then be used to solve the Dirichlet problem:

$$\boldsymbol{\sigma}'_{i+1} = \boldsymbol{\sigma}'_i - \boldsymbol{\Delta}^0 * \left[\boldsymbol{H}'.\boldsymbol{\sigma}'_i - \boldsymbol{E}'\right] \tag{A.6}$$

This iterative scheme is initialized with $\boldsymbol{\sigma}'_1 = 0$. At convergence, the macroscopic flux is determined with Eq. (25).

A faster method for computing the solution of the problem consists to consider the polarization method that uses both Green tensors and the following definition for the polarization tensor:

$$\boldsymbol{\tau}' = \delta\boldsymbol{K}'.\boldsymbol{q}', \quad \delta\boldsymbol{K}' = \boldsymbol{K}' - \boldsymbol{K}^0 \tag{A.7}$$

The polarization based iterative scheme reads:

$$\boldsymbol{\tau}'_{i+1} = \boldsymbol{\tau}'_i - \alpha\boldsymbol{K}^0.\boldsymbol{\Gamma}^0 * \left\{\boldsymbol{K}'.(\delta\boldsymbol{K}')^{-1}.\boldsymbol{\tau}'_i - \boldsymbol{E}'\right\} - \beta\boldsymbol{\Delta}^0 * \left\{(\delta\boldsymbol{K}')^{-1}.\boldsymbol{\tau}'\right\} \tag{A.8}$$

The iteration is initialized with $\boldsymbol{\tau}'_1 = 0$. In this equation $\alpha$ and $\beta$ are two coefficients, their values must be chosen such that $\alpha \in ]0, 2]$ and $\beta \in [-2, 0[$ to ensure the convergence following Monchiet and Bonnet (2012, 2013). In our applications, we use $\alpha = 1$ and $\beta = -1$.

### A.2. Neumann problem

By duality, one can easily derive the FFT based iterative scheme for the Neumann problem. The strain based iterative scheme is:

$$\boldsymbol{\varepsilon}'_{i+1} = \boldsymbol{\varepsilon}'_i - \boldsymbol{\Gamma}^0 * \left[\boldsymbol{K}'.\boldsymbol{\varepsilon}'_i - \boldsymbol{\Sigma}'\right] \tag{A.9}$$

The stress based iterative scheme is:

$$\boldsymbol{\sigma}'_{i+1} = \boldsymbol{\sigma}'_i - \boldsymbol{\Delta}^0 * \left[\boldsymbol{H}'.\boldsymbol{\sigma}'_i\right] \tag{A.10}$$

And the dual version of the polarization based iterative scheme uses the field:

$$\boldsymbol{\eta}' = \delta\boldsymbol{H}'(\boldsymbol{x}).\boldsymbol{\sigma}'(\boldsymbol{x}), \quad \delta\boldsymbol{H}'(\boldsymbol{x}) = \boldsymbol{H}(\boldsymbol{x}) - \boldsymbol{H}^0 \tag{A.11}$$

and reads;

$$\boldsymbol{\eta}'_{i+1} = \boldsymbol{\eta}'_i - \alpha\boldsymbol{H}^0.\boldsymbol{\Delta}^0 * \left\{\boldsymbol{H}'.(\delta\boldsymbol{H}')^{-1}.\boldsymbol{\eta}'_i - \boldsymbol{\Sigma}'\right\} - \beta\boldsymbol{\Gamma}^0 * \left\{(\delta\boldsymbol{H}')^{-1}.\boldsymbol{\eta}'\right\} \tag{A.12}$$

The strain, stress and polarization based iterative schemes are initialized with $\boldsymbol{\varepsilon}'_1 = 0$, $\boldsymbol{\sigma}'_1 = \boldsymbol{\Sigma}'$ and $\boldsymbol{\tau}'_1 = 0$.

## References


Auriault, J.-L., Sanchez-Palencia, E., 1977. Study of the macroscopic behavior of a saturated porous elastic medium. J. Méc. 16 (4), 575–603.

Bensoussan, A., Lions, J.-L., Papanicolau, G., 1978. Asymptotic Analysis for Periodic Structures. Elsevier.

Bhattacharya, K., Suquet, P., 2005. A model problem concerning recoverable strains of shape-memory polycrystals. Proc. R. Soc. Lond. Ser. A Math. Phys. Eng. Sci. 461 (2061), 2797–2816.

Bonnet, G., 2007. Effective properties of elastic periodic composite media with fibers. J. Mech. Phys. Solids 55 (5), 881–899.

Bornert, M., Bretheau, T., Gilormini, P., 2006. Homogenization in Mechanics of Materials. ISTE.

Eyre, D.J., Milton, G.W., 1999. A fast numerical scheme for computing the response of composites using grid refinement. Eur. Phys. J. Appl. Phys. 6 (1), 41–47.

Gélébart, L., 2020. A modified FFT-based solver for the mechanical simulation of heterogeneous materials with Dirichlet boundary conditions. C. R. Méc. 348 (8–9), 693–704.

Grimm-Strele, Hannes, Kabel, Matthias, 2021. FFT-based homogenization with mixed uniform boundary conditions. Internat. J. Numer. Methods Engrg. 122 (23), 7241–7265.

Hazanov, S., Huet, C., 1994. Order relationships for boundary conditions effect in heterogeneous bodies smaller than the representative volume. J. Mech. Phys. Solids 42 (12), 1995–2011.

Hill, R., 1952. The elastic behaviour of a crystalline aggregate.

Hill, R., 1963. Elastic properties of reinforced solids: some theoretical principles. J. Mech. Phys. Solids 11 (5), 357–372.

Huet, C., 1990. Application of variational concepts to size effects in elastic heterogeneous bodies. J. Mech. Phys. Solids 38 (6), 813–841.

Kanit, T., Forest, S., Galliet, I., Mounoury, V., Jeulin, D., 2003. Determination of the size of the representative volume element for random composites: statistical and numerical approach. Int. J. Solids Struct. 40 (13–14), 3647–3679.

Kröner, E., 1953. Das fundamental integral der anisotropen elastischen differential gleichungen. Z. Phys. 136 (4), 402–410.

Kröner, E., 1958. Berechnung der elastischen konstanten des vielkristalls aus den konstanten des einkristalls. Z. Phys. 151 (4), 504–518.

Milton, G.W., 2002. The Theory of Composites. Cambridge University Press, Cambridge.

Monchiet, V., 2015. Combining FFT methods and standard variational principles to compute bounds and estimates for the properties of elastic composites. Comput. Methods Appl. Mech. Engrg. 283, 454–473.

Monchiet, V., Bonnet, G., 2012. A polarization-based FFT iterative scheme for computing the effective properties of elastic composites with arbitrary contrast. Internat. J. Numer. Methods Engrg. 89 (11), 1419–1436.

Monchiet, V., Bonnet, G., 2013. A polarization-based fast numerical method for computing the effective conductivity of composites. Internat. J. Numer. Methods Heat Fluid Flow.

Moulinec, H., Suquet, P., 1994. A fast numerical method for computing the linear and nonlinear mechanical properties of composites. C. R. Acad. Sci. 318 (11), 1417–1423.

Moulinec, H., Suquet, P., 1998. A numerical method for computing the overall response of nonlinear composites with complex microstructure. Comput. Methods Appl. Mech. Engrg. 157 (1), 69–94.

Nguyen, M.T., To, Q.D., Monchiet, V., 2021. Derivation of FFT numerical bounds of the effective properties of composites and polycristals. Theor. Appl. Mech. Lett. 11 (2), 100236.

Salmi, M., Auslender, F., Bornert, M., Fogli, M., 2012. Apparent and effective mechanical properties of linear matrix-inclusion random composites: Improved bounds for the effective behavior. Int. J. Solids Struct. 49 (10), 1195–1211.

Sanchez-Palencia, E., 1980. Non-homogeneous media and vibration theory. Lect. Not. Phys. 127.

Timoshenko, S., Woinowsky-Krieger, S., 1959. Theory of Plates and Shells, Vol. 2. McGraw-Hill, New York.

To, Q.D., Bonnet, G., Trung, N.T., 2021. Fourier transform approach to non periodic homogenization problems in porous conductive media. Int. J. Numer. Methods Eng. 122 (18), 4864–4885.

Vondřejc, J., 2016. Improved guaranteed computable bounds on homogenized properties of periodic media by the Fourier–Galerkin method with exact integration. Internat. J. Numer. Methods Engrg. 107 (13), 1106–1135.

Wiegmann, A., 1999. Fast Elliptic Solvers on Rectangular Parallelepipeds. Technical Report, Lawrence Berkeley National Laboratory.